On the application of circuit theory and nonlinear dynamics to the design of highly efficient energy harvesting systems

On the application of circuit theory and nonlinear dynamics to the design of highly efficient energy harvesting systems

Michele Bonnin
Dept. of Electronics and Telecommunications
Politecnico di Torino
Turin, Italy
michele.bonnin@polito.it

Fabio L. Traversa
MemComputing Inc.
San Diego, CA, USA
ftraversa@memcpu.com

Fabrizio Bonani
Dept. of Electronics and Telecommunications
Politecnico di Torino
Turin, Italy
fabrizio.bonani@polito.it

***Abstract*—Ambient dispersed mechanical vibrations are a viable energy source, that can be converted into usable electric power. Ambient vibrations are random process, that can be modeled by superposition of periodic signals. When most of the energy is concentrated in a narrow frequency band, a single periodic function may be a reasonable approximation. This work shows that circuit theory, complemented with nonlinear dynamics methods, are instrumental in designing efficient energy harvesters for ambient mechanical vibrations. It is also shown that the average extracted power can be maximized by a proper load matching, and that the introduction of nonlinearities results in a larger frequency bandwidth, increasing the efficiency of the harvester at frequencies close to the resonance. Even for the nonlinear harvester, the matched load boosts the performance by a large amount.**

RELEVANT NOMENCLATURE

Symbol	*Definition*
q	electrical charge
i	current
φ	flux linkage
e	voltage
R	resistance
$G = 1/R$	conductance
L	inductance
C	capacitance
α	electromechanical gain (N/V or As/m)
$\hat{V}$, $\hat{E}$	voltage phasor
$\hat{I}$	current phasor
X, Y, Z	reactance, admittance, impedance
$Y_{in}(\omega)$, $H(\omega)$	transfer functions
ω	angular frequency
P_{out}, P_{in}	average powers
x_{rms}	root mean square of x
HB	Harmonic Balance
$\breve{\mathbf{x}}$	vector of time samples of signal $x(t)$
$\tilde{\mathbf{x}}$	vector of harmonic amplitudes of $x(t)$
$\mathbf{\Gamma}^{-1}$	DFT matrix operator
$\mathbf{\Omega}$	time derivative matrix operator

978-1-7281-7660-4/21/$31.00 2021 IEEE

I. INTRODUCTION

A. Motivation and Background

The rapid development of new technologies, e.g. the internet of things paradigm, poses a whole set of new challenges: Among others, the problem of how to supply power to networks of electronic and electro-mechanical systems that are not only miniaturized, but also wireless connected. Old fashioned solutions, like disposable batteries, are not always a valid solution, because of their limited power density, lifespan, and for the related environmental hazards and problematic disposal.

It is widely believed that systems able to scavenge energy from the surrounding environment may become a viable alternative [1]. Energy harvesting technology requires to design electro-mechanical systems, able to collect the ambient energy where and when necessary, being the ultimate power source electromagnetic radiation, solar light, temperature gradients, or mechanical vibrations. Among the many possible sources, kinetic energy is perhaps the preferred one, because of its comparatively large power density and its widespread availability. Kinetic energy exists in the form of mechanical vibrations, regular or random displacements and driving forces. It can be found in mechanical structures, due to impacts or periodic motions, in buildings and bridges, due to traffic and wind, in vehicles, due to road asperity and engine induced vibrations, as well as in the very human body motion [2].

Irrespective of the working principle, energy harvesting systems are limited by the relatively small power density of the source, and by geometric constrains. For example, a linear harvester must be carefully designed in such a way that the oscillator's resonant frequency matches the spectral range of environmental vibrations where most of the energy is concentrated. Unfortunately, the general rule is that the smaller is the size of an object, the larger its resonant frequency will be, making difficult the realization of energy harvesters that are both miniaturized, and that work efficiently at the typical frequencies of ambient mechanical vibrations.

B. Relevant Literature

A significant amount of recent literature suggests that nonlinear oscillators can perform better than linear ones [3]–[5]. When compared to their linear counterparts, nonlinear energy harvesters show a wider steady-state frequency bandwidth and may exhibit multi-stability and even chaotic dynamics, thus suggesting that they can be more efficient especially in random and non-stationary vibratory environments [6], [7].

C. Contributions and Organization

In this paper, we analyze a piezoelectric vibrational energy harvester subject to an external periodic force. First (Section II), we derive the differential equations governing the linear harvester's dynamics using Lagrange formalism, and piezoelectric material properties. Inspired by previous works [8]–[13], in Section III we use circuit theory to show that the condition for maximum power transfer cannot be achieved using a simple resistive load, but a matched resistive-reactive load must be used instead. For the nonlinear system (Section IV), we use a spectral domain technique to analyze the dynamic behavior, studying nonlinear resonances and the main bifurcation phenomena. Our analysis shows that also for the nonlinear system, the matched resistive-reactive load offers significant advantages, both in terms of output power and power efficiency, with respect to the purely resistive load.

II. Piezoelectric energy harvester: modelling

A piezoelectric energy harvester for ambient mechanical vibration scavenging, is composed by three main parts: A mechanical structure designed to capture the kinetic energy of parasitic mechanical vibration; an electrical domain for electric energy storage or electric power supply; and a piezoelectric transducer, responsible for the mechanical-to-electrical energy conversion.

A schematic representation of a piezoelectric energy harvester is shown in Fig. 1. The harvester is composed of a cantilever beam, covered by layers of piezoelectric material and fixed at one end to a moving support. An inertial mass m can be placed at the opposite end, to increase the oscillation amplitude. Vibrations of the support produce oscillations of the cantilever, inducing mechanical stress and strain in the piezoelectric material that are, in turn, converted into electrical current by a transducer. Finally the electrical current is used to supply power or recharge an electrical load.

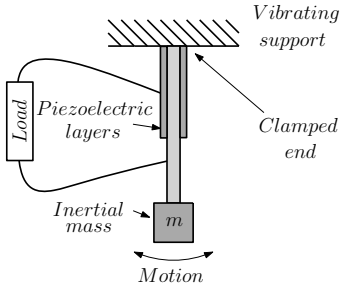

Fig. 1. Schematic representation of a piezoelectric energy harvester.

To devise an accurate mathematical model for the energy harvester, the piezoelectric transducer is considered first. The constitutive equations for a linear piezoelectric material are [14]

$$\begin{bmatrix} \boldsymbol{S} \\ \boldsymbol{D} \end{bmatrix} = \begin{bmatrix} \boldsymbol{s^E} & \boldsymbol{d} \\ \boldsymbol{d}_t & \boldsymbol{\varepsilon^T} \end{bmatrix} \begin{bmatrix} \boldsymbol{T} \\ \boldsymbol{E} \end{bmatrix} \tag{1}$$

where $\boldsymbol{S}$ and $\boldsymbol{T}$ are the mechanical strain and stress (rank two tensors), while $\boldsymbol{D}$ and $\boldsymbol{E}$ are the dielectric charge displacement and electric field strength (rank one tensors), respectively. $\boldsymbol{s^E}$ is the compliance tensor, under the condition of a constant electric field defined as strain generated per unit stress, $\boldsymbol{d}$ is the tensor of piezoelectric charge constants (rank one tensors). Finally $\boldsymbol{\varepsilon^T}$ is the absolute permittivity, e.g. the dielectric displacement per unit electric field for constant stress [15]

The linear equations (1) describe the behavior of piezoelectric material on a local scale, in terms of mechanical stress and strain, electric charge displacement and electrical field strength. A lumped parameter model can be derived in terms of global state variables, e.g. forces, displacements, currents and voltages, through spatial integration of the local variables. The corresponding equations in the quasi–static regime are

$$F_m = c\,x - \alpha\,e \tag{2}$$

$$q = \alpha\,x - C\,e \tag{3}$$

where F_m is the force applied on the mechanical part due to the electrical domain, x is the displacement, q is the electrical charge and e is the voltage. For the parameters, c is the mechanical stiffness, α is the electromechanical coupling (in N/V or As/m), and C is the electrical capacitance of the mechanical unconstrained system.

The governing equations for the mechanical and electrical parts of the harvester, can be conveniently derived using the framework of Lagrange dynamics. The Lagrangian for the mechanical part is

$$\mathcal{L}_m(x,\dot{x}) = K_m(\dot{x}) - U_m(x) = \frac{1}{2}m\dot{x}^2 - U_m(x) \tag{4}$$

where $K_m(\dot{x})$ and $U_m(x)$ are the kinetic energy and the elastic potential respectively. The corresponding Lagrange equation is

$$\frac{d}{dt}\frac{\partial \mathcal{L}_m(x,\dot{x})}{\partial \dot{x}} - \frac{\partial \mathcal{L}_m(x,\dot{x})}{\partial x} + \frac{\partial D_m(\dot{x})}{\partial \dot{x}} = F_m + f_m \tag{5}$$

where $D_m(\dot{x}) = \frac{1}{2}\gamma\dot{x}^2$ is the mechanical dissipation function with damping coefficient γ, and $f_m(t)$ represents an external force acting on the mechanical domain. If the stiffness of the piezoelectric material is neglected, the equation of motion is

$$m\ddot{x} + U'(x) + \gamma\dot{x} = f_m(t) - \alpha e \tag{6}$$

Exploiting electrical-mechanical analogies, e.g. the impedance analogy, masses are replaced by inductances, elastic potentials by capacitors[1], damping by resistors, coordinates by charges, and forces by voltages. Thus the following substitutions are

[1]For a linear elastic force with stiffness constant k, the substitution $k \to 1/C_1$ is made.

used: $m \to L_1$, $x \to q_1$, $\dot{x} \to \dot{q}_1 = i_1$, $\gamma \to R_1$, $f_m(t) \to v_s(t)$, and equation (6) is rewritten as a system of first order ODEs

$$\frac{dq_1}{dt} = i_1 \tag{7}$$

$$\frac{di_1}{dt} = -\frac{1}{L_1}U'(q_1) - \frac{R_1}{L_1}i_1 - \frac{\alpha}{L_1}e + \frac{v_s}{L_1} \tag{8}$$

The Lagrangian for the electrical part in flux coordinates is

$$\mathcal{L}_e(\varphi, \dot{\varphi}) = W_c^*(\dot{\varphi}) - W_i(\varphi) \tag{9}$$

where φ is the flux linkage, $W_c^*(\dot{\varphi})$ is the capacitive co-energy stored in the capacitors, and $W_i(\varphi)$ is the inductive energy stored in the inductors. Considering that in flux coordinates external forces are represented by currents, and taking the time derivative of (3), the Lagrange equation for the electrical domain is

$$\frac{d}{dt}\frac{\partial \mathcal{L}_e(\varphi, \dot{\varphi})}{\partial \dot{\varphi}} - \frac{\partial \mathcal{L}_e(\varphi, \dot{\varphi})}{\partial \varphi} + \frac{\partial D_e(\dot{\varphi})}{\partial \dot{\varphi}} = \alpha \dot{x} - C\dot{e} \tag{10}$$

where $D_e(\dot{\varphi}) = \frac{1}{2}G\dot{\varphi}^2$ is the electrical dissipative function and $G = 1/R$ is a conductance.

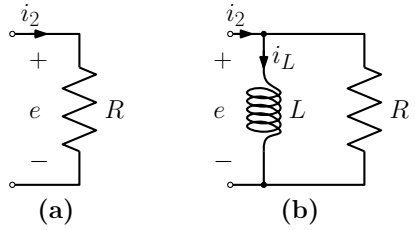

Fig. 2. **(a)** Resistive load. **(b)** Resistive-inductive load.

Two different electrical representations of the harvester load are considered: a purely resistive load and a resistive-reactive (inductive) load, as shown in Fig. 2. For the resistive load, $W_c^*(\dot{\varphi}) = 0$ and $W_i(\varphi) = 0$, and the state equations are

$$\frac{d\varphi}{dt} = e \tag{11}$$

$$\frac{de}{dt} = -\frac{G}{C}e + \frac{\alpha}{C}i_1 \tag{12}$$

Conversely, for the resistive-reactive load $W_c^*(\dot{\varphi}) = 0$, and $W_i(\varphi) = \frac{1}{2L}\varphi^2$, and the state equations become

$$\frac{d\varphi}{dt} = e \tag{13}$$

$$\frac{de}{dt} = -\frac{1}{LC}\varphi - \frac{G}{C}e + \frac{\alpha}{C}i_1 \tag{14}$$

Together with (7)-(8), equations (11)-(12) (respectively (13)-(14)) define the dynamic behavior of the equivalent circuit shown in Fig. 3, where the load is one of those shown in Fig. 2.

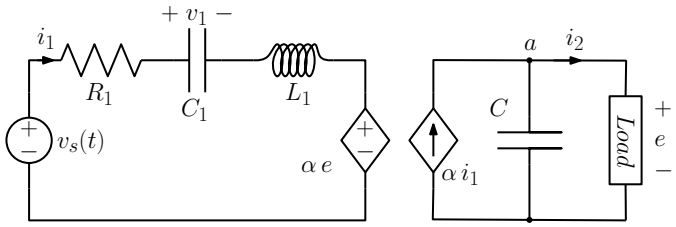

Fig. 3. Equivalent circuit for a piezoelectric energy harvester.

III. Linear harvester: transfer function and maximum power

The equivalent circuit for a linear harvester is obtained connecting linear two terminal elements. In particular, a quadratic elastic potential $U(x) = \frac{1}{2}kx^2$, where k is the elastic constant, yields a linear elastic force $F = kx$ that, according to the mechanical-electrical analogy, is represented by a linear capacitor with $k \to 1/C_1$ and $v_1 = q_1/C_1$.

For the equivalent circuit in Fig. 3, at steady state in the frequency domain, the governing equations are

$$\begin{bmatrix} R_1 + jX_1 & \alpha \\ -\alpha & j\omega C + Y_L \end{bmatrix} \begin{bmatrix} \hat{I}_1 \\ \hat{E} \end{bmatrix} = \begin{bmatrix} \hat{V}_s \\ 0 \end{bmatrix} \tag{15}$$

where $X_1 = \omega L_1 - 1/(\omega C_1)$ is the reactance of the left loop, and Y_L is the load admittance. The relevant transfer functions are

$$Y_{in}(\omega) = \frac{\hat{I}_1}{\hat{V}_s} = \frac{j\omega C + Y_L}{(R_1 + jX_1)(j\omega C + Y_L) + \alpha^2} \tag{16}$$

$$H(\omega) = \frac{\hat{E}}{\hat{V}_s} = \frac{\alpha}{(R_1 + jX_1)(j\omega C + Y_L) + \alpha^2} \tag{17}$$

Figure 4 shows a comparison of the transfer functions $H(\omega)$ for the resistive and the resistive-inductive load. For the resistive-reactive load, two different cases are considered: On the left, the left loop and the right branches of the circuit are tuned at the same resonant frequency $\omega_0 = 1/\sqrt{L_1C_1} = 1/\sqrt{LC}$. On the right, the two parts are tuned at different resonant frequencies. Parameters are normalized to yield a resonance frequency of the left loop $\omega_0 = 1/\sqrt{L_1C_1} = 1$ rad/s. The figure shows that a resistive-reactive load can be used not only to increase the output voltage at the resonant frequency, but also to increase the contribution from voltages at nearby frequencies in the case of a multi-frequency input.

In the frequency domain, the average output power delivered to the load is

$$P_{out} = \frac{1}{2}\Re[\hat{E}\,\hat{I}_2^\star] = \frac{1}{2}G|H(\omega)|^2|\hat{V}_s|^2 \tag{18}$$

where $\Re[\cdot]$ denotes the real part, and $\star$ denotes complex conjugate.

To determine the optimal load that maximizes the collected power, consider the Thevenin equivalent circuit at the load terminals. This is characterized by a Thevenin equivalent voltage source

$$\hat{V}_{eq} = \frac{\alpha}{\alpha^2 + j\omega C(R_1 + jX_1)}\hat{V}_s \tag{19}$$

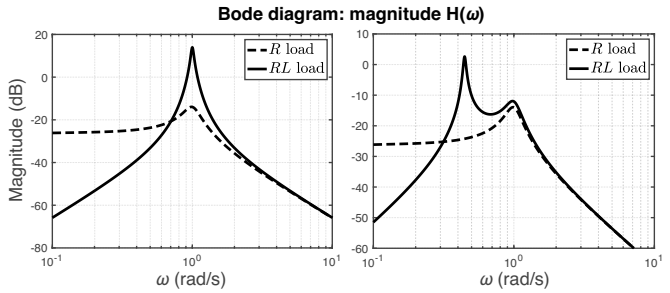

Fig. 4. Transfer function $H(\omega) = \hat{E}/\hat{V}_s$ for the equivalent circuit of Fig. 3. Normalized parameters values are: $R_1 = 0.1\ \Omega$, $L_1 = 0.4$ H, $C_1 = 2.5$ F, $\alpha = 0.1$, $R = 10\ \Omega$, $C = 5$ F. Left: $L = 0.2$ H. Right: $L = 1$ H.

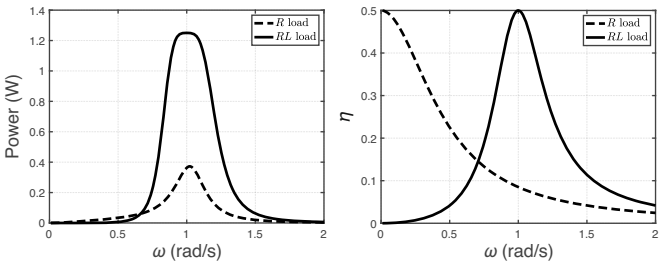

Fig. 5. Left: Average output power vs frequency for the resistive and matched RL loads. Right: power efficiency for the resistive and matched RL loads. Normalized parameters values are: $L = 0.2$H, $\alpha = 0.4$, $R = R_1/\alpha^2$, and $V_s = 1$V. Other parameters are the same as in figure 4.

and by the equivalent impedance

$$Z_{eq} = \frac{R_1 + jX_1}{\alpha^2 + j\omega C(R_1 + jX_1)} \tag{20}$$

Assuming that the left loop is tuned at the resonant frequency $\omega_0 = 1/\sqrt{L_1 C1}$ implies $X_1 = 0$ and

$$Z_{eq} = \frac{\alpha^2 R_1 - j\omega_0 C R_1^2}{\alpha^4 + \omega_0^2 C^2 R_1^2} \tag{21}$$

Maximum power is transferred from the source to the load if the load impedance is matched to Z_{eq}, that is if $Z_L = Z_{eq}^\star$. Such a condition cannot be obtained if the load is a simple resistor. Conversely, load matching can be achieved if the load is composed by an inductor L connected in parallel with a resistor R. Straightforward calculations show that maximum power transfer[2] is obtained for $R = R_1/\alpha^2$ and $L = L_1 C_1/C$, with the maximum power absorbed by the load

$$P_{max} = \frac{|\hat{V}_s|^2}{8R_1} \tag{22}$$

and the well know 50% power efficiency. Larger values for the efficiency can be obtained, but renouncing to extract the maximum power.

As it was suggested by Fig. 4, the matched RL load increases the collected power over a wide frequency interval. Figure 5 (left) shows the average output power given by (18), versus the forcing frequency for both the matched RL load and a purely resistive load. The average power delivered by the source is

$$P_{in}(\omega) = \frac{1}{2}\Re[\hat{V}_s\, \hat{I}_1^\star] = \frac{1}{2}\Re[Y_{in}(\omega)]\, |\hat{V}_s|^2 \tag{23}$$

leading to the power efficiency

$$\eta(\omega) = \frac{P_{out}(\omega)}{P_{in}(\omega)} = \frac{G\,|H(\omega)|^2}{\Re[Y_{in}(\omega)]} \tag{24}$$

shown in the right part of Fig. 5.

It is clearly seen that for the matched RL load both the maximum average output power and the maximum power efficiency are obtained at the same frequency (the resonant frequency), whereas for the resistive load the efficiency decreases as the frequency is increased.

[2]In practical applications the load resistance R_L may be fixed a priori and could not be chosen at will. Technical solutions exist to obtain load matching for fixed load. For the sake of clarity, we consider here only the simplest situation.

IV. Nonlinear energy harvester analysis

It is believed that a nonlinear energy harvester may outperform linear ones, trading off the efficiency at the resonant frequency for a larger bandwidth. An energy harvester is nonlinear when nonlinear stiffness effects are taken into account, e.g. when the elastic potential takes the form $U(x) = ax^2 + bx^4$, where a and b are real valued parameters. In the system we shall analyze, nonlinearity in the mechanical part is matched in the load, connecting a nonlinear inductor, with flux linkage-current characteristic $i_L(t) = \frac{1}{L}\varphi + \frac{1}{\widetilde{L}}\varphi^3$, in parallel with a linear resistor, so that (13)-(14) are replaced by

$$\frac{d\varphi}{dt} = e \tag{25}$$

$$\frac{de}{dt} = \frac{\alpha}{C} i_1 - \frac{1}{LC}\varphi - \frac{1}{\widetilde{L}C}\varphi^3 - \frac{G}{C}e \tag{26}$$

Consequently, the governing equations become nonlinear, non-autonomous differential equations, whose analysis is nontrivial and requires an ad hoc technique.

A. The Harmonic Balance technique

Harmonic Balance (HB) is a powerful numerical technique commonly exploited in many scientific areas, including electronic engineering, to efficiently tackle the direct determination of periodic or quasi-periodic solutions of dynamical systems, thus avoiding the computation of the transient part of the solution altogether. Essentially, HB transforms the system differential equations into an algebraic systems whose unknowns are the coefficients of the Fourier series representing the steady-state solution [16].

In order to introduce the notation first, a scalar real function $x(t)$ is considered, represented in the frequency domain by means of a (truncated) exponential Fourier series

$$x(t) = \sum_{h=-N_{\mathrm{H}}}^{N_{\mathrm{H}}} \tilde{x}_h\ \mathrm{e}^{jh\omega_0 t} \tag{27}$$

where $\tilde{x}_h$ is the h-th harmonic amplitude associated to the (angular) frequency $h\omega_0 = h2\pi/T$ (h-th harmonic). As $x(t)$

is real, $\tilde{x}_{-h} = \tilde{x}_h^\star$, so that the Fourier series is fully defined by $2N_\mathrm{H}+1$ real coefficients. The numerical implementation of HB is more effectively carried out replacing (27) by the trigonometric series representation [17], however for theoretical developments the more compact exponential form is preferred here.

After discretizing the $]0,T]$ fundamental period with a set of $2N_\mathrm{H}+1$ time samples t_k ($k = 1,\dots,2N_\mathrm{H}+1$), the time sampled variable are collected into vector $\breve{\mathbf{x}} = [x(t_1), x(t_2), \dots, x(t_{2N_\mathrm{H}+1})]^\mathrm{T}$, which in turn is related to the collection of harmonic amplitudes $\tilde{\mathbf{x}} = [\tilde{x}_{-N_\mathrm{H}}, \tilde{x}_{-N_\mathrm{H}+1}, \dots, \tilde{x}_0, \dots, \tilde{x}_{N_\mathrm{H}}]^\mathrm{T}$ by means of the discrete Fourier transform (DFT) invertible linear operator $\mathbf{\Gamma}^{-1}$

$$\breve{\mathbf{x}} = \mathbf{\Gamma}^{-1}\tilde{\mathbf{x}} \Longleftrightarrow \tilde{\mathbf{x}} = \mathbf{\Gamma}\breve{\mathbf{x}}. \tag{28}$$

Clearly for $N_\mathrm{H} \to \infty$, $\mathbf{\Gamma}^{-1}$ is the matrix representation of the operator defining the Fourier series representation of a T-periodic function.

In the frequency domain, for the exponential series a diagonal matrix $\mathbf{\Omega} \in \mathbb{C}^{(2N_\mathrm{H}+1)\times(2N_\mathrm{H}+1)}$ proportional to ω_0 represents the time derivative [16]

$$\tilde{\dot{\mathbf{x}}} = \mathbf{\Gamma}\breve{\dot{\mathbf{x}}} = \mathbf{\Omega}\tilde{\mathbf{x}} \tag{29}$$

where $\dot{\alpha}(t) = \mathrm{d}\alpha/\mathrm{d}t$.

Moving now to the vector case, considering $\mathbf{x}(t) \in \mathbb{R}^n$ (28) and (29) are easily generalized by expanding each time sample $\alpha(t_i)$ into a vector $\mathbf{x}(t_i) \in \mathbb{R}^n$, whose collection becomes $\breve{\mathbf{x}} = [\mathbf{x}^\mathrm{T}(t_1), \mathbf{x}^\mathrm{T}(t_2), \dots, \mathbf{x}^\mathrm{T}(t_{2N_\mathrm{H}+1})]^\mathrm{T} \in \mathbb{R}^{n(2N_\mathrm{H}+1)}$. Correspondingly, the frequency domain representation is $\tilde{\mathbf{x}} = [\tilde{\mathbf{x}}^\mathrm{T}_{-N_\mathrm{H}}, \dots, \tilde{\mathbf{x}}^\mathrm{T}_0, \dots, \tilde{\mathbf{x}}^\mathrm{T}_{N_\mathrm{H}}]^\mathrm{T} \in \mathbb{C}^{n(2N_\mathrm{H}+1)}$. In this way, equations (28) and (29) can formally be extended by defining two block diagonal matrices $\mathbf{\Gamma}_n^{-1}$ and $\mathbf{\Omega}_n$ built replicating n times the fundamental operators $\mathbf{\Gamma}^{-1}$ and $\mathbf{\Omega}$

$$\breve{\mathbf{x}} = \mathbf{\Gamma}_n^{-1}\tilde{\mathbf{x}} \qquad \tilde{\dot{\mathbf{x}}} = \mathbf{\Omega}_n\tilde{\mathbf{x}}. \tag{30}$$

Let us now apply these concepts to the case of a vector dynamical system forced by a T-periodic source term $\mathbf{s}(t)$:

$$\dot{\mathbf{x}}(t) = \mathbf{f}(\mathbf{x}(t)) + \mathbf{s}(t) \tag{31}$$

After time-sampling and DFT transformation, (31) becomes

$$\mathbf{\Omega}_n\tilde{\mathbf{x}} = \tilde{\mathbf{f}}(\mathbf{\Gamma}_n^{-1}\tilde{\mathbf{x}}) + \tilde{\mathbf{s}} \tag{32}$$

where $\tilde{\mathbf{f}}$ represents the collection of harmonic amplitudes for the T periodic function $\mathbf{f}(\mathbf{x}(t))$.

Algebraic equation (32) can be solved numerically exploiting the Newton algorithm, and specialized techniques have also been developed for specific analyses, such as the stability assessment of the resulting solution [17]–[20].

B. Nonlinear piezoelectric energy harvester analysis

The HB technique has been applied to analyze the nonlinear energy harvester described by the ODE (7)-(8) (with $U(q_1) = \frac{q_1}{C_1} + \frac{q_1^3}{\widetilde{C}_1}$), and (25)-(26). To speed up the procedure, the HB technique has been applied in conjunction with a continuation method, using the solution for a certain value of the forcing frequency as the initial condition for the Newton algorithm applied to the following value of this parameter. It is worth mentioning that another advantage of the HB is that it permits to detect both stable and unstable solutions, including limit cycle of saddle type that cannot be detected through numerical integration, neither forward nor backward in time.

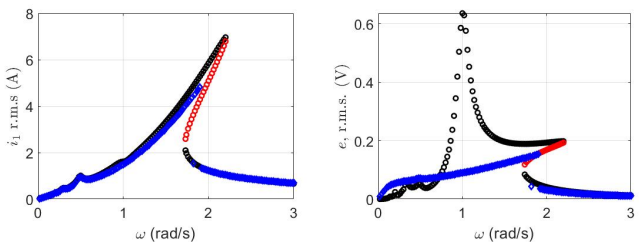

Fig. 6. r.m.s. value for the input current $i_1(t)$ (left) and the output voltage $e(t)$ (right) vs the forcing frequency. Blacks circles are asymptotically stable solutions; red circles are unstable solution of saddle type; blue diamonds are stable solutions for the resistive load case, shown for comparison. Parameters are $\widetilde{L} = 10$ H V^{2}s^2, $\widetilde{C}_1 = 10$ F A^{2}s^2, $\alpha = 0.1$, other parameters are the same of figures 4-5. HB simulation performed with $N_\mathrm{H} = 100$ harmonics.

Figure 6 show the root mean square [3] (r.m.s.), value for the input current $i_1(t)$ and the output voltage $e(t)$, as functions of the forcing frequency. It can be seen that the system exhibits the following behavior: For small value of ω, there is a unique, asymptotically stable periodic solution (black circles). As the forcing frequency is increased, the r.m.s. values increase, implying that the amplitude of the periodic solution increases. At the critical value $\omega_{SN_1} \approx 1.71$ rad/s, a saddle node bifurcation, identified by a Floquet multiplier equal to one, occurs. Two new periodic solutions emerge: the smaller is asymptotically stable, whereas the larger is unstable of saddle type. At the critical frequency $\omega_{SN_2} \approx 2$ rad/s the unstable solution and the large, stable periodic solution collide, and disappear through a second saddle-node bifurcation. The small, stable limit cycle remains as the unique solution. For the sake of comparison, the r.m.s. values for the purely resistive load are also shown. These values have been obtained through numerical integration and averaging of equations (7)-(8) and (11)-(12). It can be seen that, especially for the output voltage, the matched RL load offers much better performance over a wide frequency range.

The r.m.s. values of i_1 and e allow for an easy calculation of the average injected and extracted power. For the equivalent circuit shown in Fig. 3, the average power transferred to the load is

$$P_{out} = \frac{G}{T}\int_0^T e(t)^2\,dt = Ge_{rms}^2 \tag{33}$$

[3]The r.m.s. value of a T-periodic function $x(t)$ is defined as

$$x_{rms} = \sqrt{\frac{1}{T}\int_0^T [x(t)]^2 dt}$$

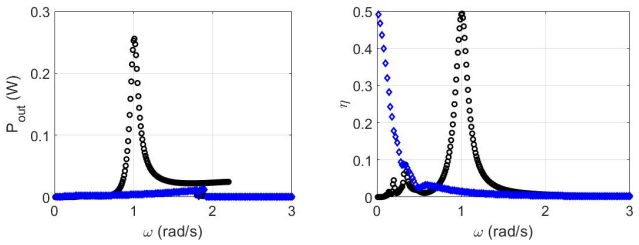

Fig. 7. Average output power (left) and power efficiency (right) vs forcing frequency. Black circles are for the matched RL load; blue diamonds are for the resistive load. Parameters are the same of figure 6.

For the input power, using Tellegen's theorem, we have

$$P_{in} = \frac{1}{T}\int_0^T v_s(t) i_1(t)\, dt = R_1 i_{1,rms}^2 + G\, e_{rms}^2 \qquad (34)$$

where we used the fact that the controlled sources do not dissipate power, as they only transfer it from the left loop to the right branches, and that reactive elements (inductors and capacitors) do not absorb active power, but only reactive power.

Figure 7 shows the average power transferred to the load (on the left) and the power efficiency $\eta = P_{out}/P_{in}$ as functions of the forcing frequency. Both the matched RL load and the purely resistive load are shown. It is evident that, for the average output power, the matched RL load outperforms the resistive load over a wide frequency band. Moreover, for these parameter values, the maximum efficiency is achieved at the resonant frequency, whereas for the resistive load the efficiency is a decreasing function of the forcing frequency.

V. Conclusions

Ambient dispersed mechanical vibrations are a viable energy source, that can be converted into usable electrical power using piezoelectric energy harvesters. In general, ambient vibrations are random processes, that can be modeled as a superposition of periodic functions, with random amplitudes and frequencies. When most of the power is concentrated in a narrow frequency band, however, a single periodic function may be used as a reasonable approximation.

In this work, we have analyzed a piezoelectric energy harvester subject to a periodic external force. The differential equations describing the harvester's dynamics have been derived applying the Lagrange approach to electro-mechanical systems, and an equivalent circuit model has been devised exploiting mechanical-to-electrical analogies. Application of circuit theory has allowed to prove that maximum power can be transferred to the load by a proper load matching. In the linear case, matching is obtained by connecting a reactive element in parallel with a resistive load. Under resonant conditions, the harvester becomes equivalent to a pair of coupled oscillators, running at the same frequency. The well known 50% efficiency under maximum power transfer conditions is achieved at the same resonant frequency.

For a nonlinear harvester, we have shown that the system can be efficiently analyzed applying a frequency domain technique, namely the harmonic balance. The occurrence of nonlinear resonance and bifurcation phenomena has been illustrated and analyzed. Similarly to the linear case, modification of the load with a reactive component increases the average power transferred to the load and the power efficiency with respect to the simple resistive load case.

References

[1] X. Lu, P. Wang, D. Niyato, D. I. Kim, and Z. Han, "Wireless networks with RF energy harvesting: A contemporary survey," *IEEE Communications Surveys & Tutorials*, vol. 17, no. 2, pp. 757–789, 2015.

[2] A. Khaligh, P. Zeng, and C. Zheng, "Kinetic energy harvesting using piezoelectric and electromagnetic technologiesstate of the art," *IEEE transactions on industrial electronics*, vol. 57, no. 3, pp. 850–860, 2009.

[3] F. Cottone, H. Vocca, and L. Gammaitoni, "Nonlinear energy harvesting," *Physical Review Letters*, vol. 102, no. 8, p. 080601, 2009.

[4] Y. Fu, H. Ouyang, and R. B. Davis, "Nonlinear dynamics and triboelectric energy harvesting from a three-degree-of-freedom vibro-impact oscillator," *Nonlinear Dynamics*, vol. 92, no. 4, pp. 1985–2004, 2018.

[5] M. Bonnin, F. L. Traversa, and F. Bonani, "Analysis of influence of nonlinearities and noise correlation time in a single-DOF energy-harvesting system via power balance description," *Nonlinear Dynamics*, vol. 100, no. 1, pp. 119–133, mar 2020.

[6] M. Xu and X. Li, "Two-step approximation procedure for random analyses of tristable vibration energy harvesting systems," *Nonlinear Dynamics*, vol. 98, no. 3, pp. 2053–2066, 2019.

[7] Z. Yan, W. Sun, M. R. Hajj, W. Zhang, and T. Tan, "Ultra-broadband piezoelectric energy harvesting via bistable multi-hardening and multi-softening," *Nonlinear Dynamics*, vol. 100, p. 10571077, 2020.

[8] H. Abdelmoula and A. Abdelkefi, "Ultra-wide bandwidth improvement of piezoelectric energy harvesters through electrical inductance coupling," *The European Physical Journal Special Topics*, vol. 224, no. 14-15, pp. 2733–2753, 2015.

[9] B. Yan, S. Zhou, and G. Litak, "Nonlinear analysis of the tristable energy harvester with a resonant circuit for performance enhancement," *International Journal of Bifurcation and Chaos*, vol. 28, no. 07, p. 1850092, 2018.

[10] D. Huang, S. Zhou, and G. Litak, "Analytical analysis of the vibrational tristable energy harvester with a RL resonant circuit," *Nonlinear Dynamics*, vol. 97, no. 1, pp. 663–677, 2019.

[11] S. Zhou and T. Yu, "Performance comparisons of piezoelectric energy harvesters under different stochastic noises," *AIP Advances*, vol. 10, no. 3, p. 035033, 2020.

[12] T. Yu and S. Zhou, "Performance investigations of nonlinear piezoelectric energy harvesters with a resonant circuit under white gaussian noises," *Nonlinear Dynamics*, vol. 103, no. 1, pp. 183–196, 2021.

[13] M. Bonnin, F. L. Traversa, and F. Bonani, "Leveraging circuit theory and nonlinear dynamics for the efficiency improvement of energy harvesting," *Nonlinear Dynamics*, feb 2021.

[14] "IEEE standard on piezoelectricity," 1988. [Online]. Available: https://ieeexplore.ieee.org/servlet/opac?punumber=2511

[15] S. Priya and D. J. Inman, *Energy harvesting technologies*. Springer, 2009, vol. 21.

[16] K. S. Kundert, A. L. Sangiovanni-Vincentelli, and J. K. White, *Steady-State Methods for Simulating Analog and Microwave Circuits*. Springer, Dec. 2010.

[17] F. L. Traversa, F. Bonani, and S. D. Guerrieri, "A frequency-domain approach to the analysis of stability and bifurcations in nonlinear systems described by differential-algebraic equations," *International Journal of Circuit Theory and Applications*, vol. 36, no. 4, pp. 421–439, 2008.

[18] F. L. Traversa and F. Bonani, "Improved harmonic balance implementation of floquet analysis for nonlinear circuit simulation," *AEU - International Journal of Electronics and Communications*, vol. 66, no. 5, pp. 357–363, may 2012.

[19] F. Traversa and F. Bonani, "Frequency-domain evaluation of the adjoint floquet eigenvectors for oscillator noise characterisation," *IET Circuits, Devices & Systems*, vol. 5, no. 1, p. 46, 2011.

[20] M. Bonnin, F. Traversa, and F. Bonani, "Efficient spectral domain technique for the frequency locking analysis of nonlinear oscillators," *The European Physical Journal Plus*, vol. 133, no. 7, pp. 1–12, 2018.